Research Square

Preprints are preliminary reports that have not undergone peer review.
They should not be considered conclusive, used to inform clinical practice,
or referenced by the media as validated information.

Cryptic recycling of continental crust during subduction of extended arcs and margins in Paleozoic Japan

Daniel Pastor-Galán

dpastorgalan@csic.es

CSIC https://orcid.org/0000-0002-0226-2739

Ariuntsetseg Ganbat

Georg-August-Universität Göttingen

Atsushi Miyashita

The Open University of Japan https://orcid.org/0000-0003-4639-0385

Christopher Spencer

Queen's University https://orcid.org/0000-0003-4264-3701

Pol Vilanova Catalá

Departament de Mineralogia, Petrologia i Geologia Aplicada, Universitat de Barcelona, Barcelona

Noreen Evans

Curtin University https://orcid.org/0000-0002-7615-8328

Tatsuki Tsujimori

Tohoku University https://orcid.org/0000-0001-9202-7312

Article

Keywords:

Posted Date: August 14th, 2026

DOI: https://doi.org/10.21203/rs.3.rs-10367757/v1

License: This work is licensed under a Creative Commons Attribution 4.0 International License.
Read Full License

Additional Declarations: There is **NO** Competing Interest.

Abstract

Continental crust is the archive of Earth's geological history, but its preservation is strongly imbalanced: although more than 65% of the present continental mass formed before 3 Ga, less than 5% of exposed crust is older than this age. Mass balance estimates indicate that two to four times the present continental mass has been recycled into the mantle over Earth history (6 to 12 × 10^{22} kg). Proposed recycling processes, including subduction erosion, sediment subduction, delamination, and continental subduction, collectively account for only a fraction of the flux required to maintain long-term mass balance. Here, we document an episode of efficient continental crust recycling along the Paleozoic margin of Japan. Zircon geochemistry from rare pre-Mesozoic granitoids records one, and possibly two, Paleozoic episodes of continental destruction. These data record a shift from mixed to juvenile isotopic signatures, consistent with the loss of an evolved crustal component in magma generation and its replacement by mantle-derived magmatism. We interpret this transition as recording efficient recycling of fragmented continental crust during back-arc extension and subsequent subduction. This process may represent an efficient yet cryptic pathway for continental crust recycling and a significant, previously underappreciated component of the long-term crustal cycle.

Introduction

In classical plate tectonic frameworks, continents are often treated as permanent entities drifting atop the mantle[1]. However, the geological record tells a different story: less than 5% of the exposed continental crust is older than 3 Ga [2–4], whereas geochemical models indicate that more than 65% of the present continental mass formed prior to 3 Ga [5]. This mismatch implies that vast volumes of continental material have been removed from the crust and recycled into the mantle[7,1]. Mass balance calculations estimate that 6–12 × 10^{22} kg of continental crust has been recycled throughout Earth's history. This is equivalent to two to four times the current mass of the continents [6,7]. The disappearance of "lost continents" highlights a fundamental bias in the geological record: crust formation and preservation are well recorded, whereas crustal destruction is cryptic and poorly recorded. As a result, plate reconstructions, geodynamic models, and paleoclimate studies may systematically underestimate large volumes of continental crust, especially in deep time, obscuring key processes that have shaped the long-term evolution of the Earth.

Several mechanisms have been proposed for continental crust recycling: subduction erosion (~1.5 km^3/yr), sediment subduction (~1.5 km^3/yr), lower crustal delamination (~1.1 km^3/yr), and continental subduction (average of 0.4 km^3/yr with peaks of ~2.5 km^3/yr during major orogenesis)[8–18] (Fig. 1). A significant fraction of this material, at least 20%, never reaches the mantle and instead melts and reaccretes to the crust[19,20]. Even allowing for substantial uncertainties and variability, the combined contribution of all mechanisms (~3.6 km^3/yr) falls short by at least a factor of two compared to what would be required to resolve the global crustal mass deficit through timescales (7.4 to 14.8 km^3/yr)[6].

Here we investigate the Paleozoic Japan convergent margin (Fig. 2, EDF 1), where rare pre-Mesozoic granitoids preserve a fragmentary record of crustal evolution. Zircon U–Pb geochronology, Lu–Hf isotopes, and trace element geochemistry identify a transition from radiogenically enriched to strongly depleted magmatism. We interpret this shift as reflecting the progressive removal of continental lithosphere from the magmatic system during rollback-driven extension and subsequent subduction of hyperextended crustal fragments. If correct, this process represents an efficient but largely cryptic mechanism of continental crust recycling with implications for Earth's long-term crustal mass balance.

The Phanerozoic Japanese crustal record

Japan records at least ~600 million years of subduction history[13]. The continental crust of present-day Japan is widely interpreted to derive from fragments of the North and/or South China [21–23], rifted during the breakup of Rodinia and the opening of the Panthalassa Ocean[24]. Following an uncertain Precambrian interval, subduction initiated beneath proto-Japan as recorded by arc granitoids and serpentinized mantle wedge peridotites with Cambrian jadeitites[25,26], establishing a long-lived convergent margin that persists to the present day. The only well-documented continent–continent collision is preserved in the Hida Belt[27], emplaced during the Triassic amalgamation of the North and South China cratons[28]. In contrast, much of Japan’s evolution reflects sustained oceanward subduction and accretion, including incorporation of intraoceanic arcs, as exemplified by the modern Izu–Bonin system[29].

Paleozoic ophiolites record multiple stages of oceanic lithosphere formation and subduction along this evolving margin. In Northeast Japan, the Hayachine–Miyamori complexes define an Ordovician (~480–460 Ma) arc–back-arc system[30]. In Southwest Japan, ophiolitic fragments span a broader range[31]: the Oeyama ophiolite formed during the Cambrian–Early Ordovician (~540–530 Ma) in a supra-subduction setting, whereas the Yakuno ophiolite records Permian (~290–240 Ma) arc–back-arc magmatism (Fig. 2, EDF 1). The Oeyama was tectonically thrusted over the Permian accretionary complex and the Maizuru Belt which contains Permian arc sequences but also inherited continental material with Ordovician to Paleoproterozoic zircon ages, indicating preservation of an older cratonic fragment within the orogenic collage. Together, these units document a spatially heterogeneous and long-lived history of subduction, arc development and tectonic assembly.

Despite this prolonged history, most of the Japanese crust is Cretaceous or younger [32]. Seismic data indicate that pre-Cretaceous rocks are largely restricted to shallow roof pendants[33], and pre-Jurassic plutonic rocks are remarkably scarce. Only small remnants of ~500–400 Ma granitoids are preserved as blocks in the Southern Kitakami Mountains or fragments within belts such as Kurosegawa, while Carboniferous–Permian intrusions are rare and Triassic plutonism is largely related to the China blocks collision and therefore confined to the Hida Belt. This scarcity is widely attributed to long-term tectonic erosion and recycling of arc crust into the mantle, obscuring much of Japan’s early evolution[24]. Detrital zircon records support this view, showing episodic magmatic pulses interspersed with quiescent

intervals and an overall shift toward more juvenile isotopic signatures through time, punctuated by episodes of enhanced crustal loss[13].

Pre-Mesozoic intrusive record on Northeast Japan

Pre-Mesozoic intrusive rocks in Japan are rare and typically poorly exposed, occurring either as isolated fault-bounded bodies or as small remnants enclosed within younger Mesozoic granitoids. To characterise this fragmentary magmatic record, we sampled granitoids from Northeast Japan, including both in situ intrusions and cobbles preserved in sedimentary conglomerates that provide independent depositional age constraints. The dataset comprises two Cambrian samples previously interpreted as part of the Japanese crust[25], three Ordovician–Silurian samples, including a trondhjemite from an ophiolitic complex[34] and two from an early Silurian continental arc[13], and six Carboniferous–Permian plutonic rocks linked to continental arc magmatism[24]. Zircon grains (~50 per sample) were analysed for U–Pb ages, Lu–Hf isotopic composition, and trace elements (including REE, Sr, Y, P and Al). Only the most reliable analyses, screened for inclusions, mixed domains, and discordance (<5% for ages; <10% for Hf), were retained to ensure robust age and isotopic interpretations.

Cambrian samples (Fig. 2, in detailed in Supplementary file) yielded tightly clustered ages of ~500 Ma. These rocks show consistently positive εHf values (+8 to +15), indicating derivation from a dominantly juvenile, mantle-derived source with limited involvement of older crust. The Ordovician trondhjemite (~470 Ma) from the Hayachine ophiolitic complex shows strongly juvenile εHf signatures (+12 to +16) consistent with a depleted mantle source (Fig. 2). These samples are considered part of an intraoceanic or previously extended arc[35]. In contrast the Ordovician-Silurian granitoids sampled yielded ~440 Ma and evolved εHf values (−9 to +5), consistent with significant crustal involvement and a continental arc origin[13]. Carboniferous–Permian plutonism (300- 280 Ma) is characterized by uniformly positive εHf values (+9 to +15), indicating a return to predominantly juvenile, mantle-derived sources.

Zircon trace-element systematics indicate systematic temporal variations in magma chemistry across the Paleozoic (Fig. 3). The Ordovician–Silurian continental arc is characterized by the lowest Eu/Eu*, highest U/Yb, relatively reduced conditions (FMQ to FMQ−2), and mostly lower crystallization temperatures (≤800 °C), consistent with evolved, more differentiated magma. Cambrian zircons display intermediate characteristics, whereas the Carboniferous–Permian suites exhibit higher Eu/Eu*, lower U/Yb, higher Ce/Yb, and a subset of grains plotting within the mantle zircon array, indicating the strongest mantle contribution. Zircon oxybarometry further shows that the Carboniferous–Permian suites crystallized under more oxidizing conditions (FMQ to FMQ+2) and at higher temperatures (>900 °C), than the Cambrian arc.Taken together, the εHf and zircon trace-element spectra describe a progression where the Cambrian-Ordovician arc magmas are moderately oxidized and isotopically juvenile, but retaining a crustal trace-element signature (high U/Yb), consistent with arc magmatism built on, or contaminated by, pre-existing crust. The Ordovician–Silurian arc was relatively cool, reduced, plagioclase-controlled, and contaminated, representing an evolved continental-arc endmember. The Carboniferous-Permian magmas were hotter, more oxidized, and isotopically depleted (εHf +9 to +15;

Fig. 4), relative to the Ordovician-Silurian suite. These observations indicate a fundamental change in magma source and differentiated through a deep, amphibole-bearing root in which plagioclase was suppressed, consistent with their high whole-rock Sr/Y (EDF 2). From them three samples (Fig. 3) define the hottest, most oxidized compositions, indicating predominantly hot, mantle-derived magma emplaced at shallow levels.

Crustal Recycling at the Paleozoic Japanese Margin of Panthalassa

Our results require a fundamental change in magma source between Ordovician-Silurian and Carboniferous-Permian magmatism. The disappearance of evolved isotopic signatures, together with the appearance of hotter, more oxidized and mantle-dominated magmas, is difficult to reconcile with simple steady-state arc evolution[36]. We propose that continental crust is most efficiently recycled when it is first thinned and fragmented during back-arc extension, enabling its subduction together with oceanic lithosphere. Alternative explanations include changes in mantle source composition, variations in crustal assimilation, or migration of magmatism to a different segment of the convergent margin. Although these processes may contribute locally, none readily explains the simultaneous isotopic, trace-element, and thermal evolution observed across multiple intrusive suites. Instead, the simplest explanation is a fundamental reduction in the availability of evolved continental crust beneath the arc.

Unlike accretionary orogens such as those of Central Asia and eastern Australia, which are characterized by progressive crustal growth[37,38], the Japanese accretionary system records destruction of evolved crust followed by renewal of the lithosphere during the Late Paleozoic. Juvenile magmatism associated with lithospheric thinning has been also documented in the South China craton[21,22], commonly interpreted as the cratonic counterpart to the proto-Japan arc[13,25]. The strongly εHf signatures observed in both regions are consistent with asthenospheric upwelling and enhanced mantle input during episodes of crustal thinning, reflecting dispersal and removal of older continental lithosphere.

Our model predicts four independent observations: 1) evidence for Devonian-Carboniferous slab rollback and back-arc extension, 2) preservation of hyperextended continental fragments or their remnants (Fig. 4)[39,40], 3) increased mantle-derived magmatism accompanying extension, and 4) subsequent convergence capable of subducting the extended crust. Available geological observations from Paleozoic Japan are consistent with each of these predictions[13]. This interpretation is consistent with the presence of arc–back-arc lithologies such as the Yakuno ophiolite, and with the preservation of isolated continental fragments such as those within the Maizuru Belt (Fig. 2; EDF 1).

Recycling was completed during subsequent convergence, when back-arc basin closure leads to subduction of the hyperextended domain, including dispersed continental fragments and portions of the juvenile arc. At this stage, large volumes of continental material are transferred into the mantle with minimal preservation in the geological record. Although continental crust is buoyant at shallow mantle levels, its density severely increases due to high-pressure phase transformations and at depths of ~270 km, continental materials are denser than the surrounding mantle[41] allowing it to become

negatively buoyant and sink potentially to transition zone depths or beyond[42]. In this context, the Yakuno ophiolite likely represents transitional arc–back-arc crust emplaced during basin closure, whereas the Maizuru Belt preserves only limited remnants of the pre-existing continental crust[43].

Although best recorded during the Carboniferous–Permian transition, the scarcity and isotopic variability (εHf +8 to +16) of Cambrian–Silurian rocks, typically interpreted as products of intraoceanic arc accretion or back-arc closure[34,35], suggest that similar processes may have operated earlier in the Paleozoic. Their limited preservation is consistent with repeated cycles of arc extension, fragmentation, and recycling, which preferentially remove the crustal domains they generate. Such cryptic recycling provides a mechanism for efficiently transferring continental material into the mantle and contributes to the long-term imbalance between crust generation and preservation.

Constraining the Missing Flux of Continental Crust

Rather than derive a precise global recycling rate, our objective is to assess whether this mechanism is potentially large enough to influence long-term continental mass balance. The imbalance between continental crust production and preservation[2] requires efficient mechanisms capable of removing large volumes of crust from the surface (Fig. 1). Estimates of recycling flux based on subduction erosion, sediment subduction and delamination fall well short of that required to maintain long-term mass balance, suggesting that additional pathways must contribute to continental crust loss. Quantifying the flux of continental crust recycled into the mantle is inherently challenging because such processes lead to the near-complete removal of the crust involved. As a result, the most efficient recycling mechanisms may be those least likely to be preserved, and any estimates must rely on fragmentary evidence and indirect constraints. Consequently, reconstructed fluxes should be regarded as minimum values, and even conservative estimates provide important first-order constraints.

Extensional processes such as back-arc opening and rifting generate thinned continental domains that may become mechanically coupled to surrounding oceanic lithosphere as “orphaned” fragments (e.g., Zealandia and Mauritia)[39,40,44]. Once incorporated into convergent systems, these fragments can be subducted with limited upper-plate deformation and minimal preservation, providing an efficient yet largely cryptic pathway for transferring continental crust to the mantle. This process, as documented in the Paleozoic Japanese arc, is likely to operate more widely than is currently recognized.

To estimate a minimum flux associated with this process, we consider the present-day extent of identified hyperextended continental crust preserved within oceanic domains (EDF 5), deliberately excluding the growing evidence for smaller, but more widespread continental slivers[45]. Assuming an average crustal thickness of ~15 km and that ~80% of oceanic lithosphere is subducted over ~100 Myr[46], a first-order extrapolation yields a gross flux of ~1.5 $km^3\,yr^{-1}$. If approximately 50% of this material is retained within the crust through accretion, melting or relamination (Fig. 1), the net flux to the mantle remains on the order of ~0.75 $km^3\,yr^{-1}$. Although this calculation is intentionally conservative and

associated with substantial uncertainty, it demonstrates that subduction of hyperextended continental fragments is unlikely to be negligible in global crustal recycling budgets.

Our results suggest that continental destruction is not restricted to collisional orogens or subduction erosion at active margins, but may instead represent an intrinsic stage in the tectonic evolution of long-lived convergent margins. Episodes of rollback-driven extension create mechanically weakened continental fragments that become susceptible to later subduction, effectively erasing evidence of their existence. If widespread, this process implies that the preserved continental record is not simply incomplete but systematically biased toward crustal survival, with episodes of continental destruction preferentially erased from the geological archive.

Online Methods

1. **Laser ablation split stream analysis (LASS-ICPMS) of Hf isotopes (LA-MC-ICPMS) and U-Pb ages (LA-QQQ-ICPMS)**

Zircon crystals were mounted in 1” epoxy rounds and polished to reveal internal surfaces. Hafnium isotopes and U-Pb ages in zircon were simultaneously measured by laser ablation split stream at the Geohistory Facility in the John de Laeter Centre across three analytical sessions. Grains were ablated using a Resonetics RESOlution SE 193nm laser incorporating a dual volume S155 sample cell, coupled to a Nu Plasma II multi-collector inductively coupled plasma mass spectrometer (MC-ICPMS) for Hf isotope determination and an Agilent 8900 triple quadrupole inductively coupled plasma mass spectrometer (QQQ-ICPMS) for age determination. Following two cleaning pulses and a 40s period of background analysis, samples were spot ablated for 35s at a 10Hz repetition rate using a 38µm beam and laser energy at the sample surface of 2.2 J cm^{-2}. An additional 15s of baseline was collected after ablation. The sample cell was flushed with ultrahigh purity He (320 mL min^{-1}) and N_2 (1.2 mL min^{-1}) and high purity Ar was employed as the plasma carrier gas, split to each mass spectrometer.

For Hf isotope analysis, all isotopes (^{180}Hf, ^{179}Hf, ^{178}Hf, ^{177}Hf, ^{176}Hf, ^{175}Lu, ^{174}Hf, ^{173}Yb, ^{172}Yb and ^{171}Yb) were counted on the Faraday collector array. Time resolved data was baseline subtracted and reduced using Iolite (DRS after Woodhead et al., 2004[54]), where ^{176}Yb and ^{176}Lu were removed from the 176 mass signal using $^{176}Yb/^{173}Yb = 0.7962$[55] and $^{176}Lu/^{175}Lu = 0.02655$[55] with an exponential law mass bias correction assuming $^{172}Yb/^{173}Yb = 1.35274$[55]. An effective $^{176}Yb/^{173}Yb$ correction factor was determined for each session by iteratively adjusting the $^{176}Yb/^{173}Yb$ ratio until standard corrected ratios on secondary zircon reference materials with varying Yb content yielded values within the recommended range. No correlation was apparent between the abundance of interfering isotopes (Yb or Lu) and corrected $^{176}Hf/^{177}Hf$ ratios. The interference corrected $^{176}Hf/^{177}Hf$ was normalized to $^{179}Hf/^{177}Hf = 0.7325$[56] for mass bias correction. Zircon from the Mud Tank carbonatite locality was analysed together with the samples in each session to provide standard referenced $^{176}Hf/^{177}Hf$ ratios (Table EDF-6). In all cases, Mud Tank analyses reproduced the recommended value (0.282505 ± 44[57]) within uncertainty.

Data for secondary standards is also provided in Table EDF-6. All standards reproduced accepted values within uncertainty for each session. In addition, the corrected $^{178}Hf/^{177}Hf$ ratio was calculated to monitor the accuracy of the mass bias correction and yielded a weighted mean of 1.4670426 ± 0.0000088 (2sigma; MSWD = 0.64), which is within the range of values reported by Thirlwall and Anczkiewicz[58]. Calculation of εHf values employed the decay constant of Scherer et al.[59] and the Chondritic Uniform Reservior (CHUR) values of Blichert-Toft and Albarède[60].

Ages were simultaneously measured on the aerosol split using LA-Q-ICP-MS analysis and the following isotopes were monitored for 0.01-0.02 s each: ^{202}Hg, ^{204}Pb, ^{206}Pb, ^{207}Pb, ^{208}Pb, ^{232}Th, and ^{238}U. The primary dating reference materials used in this study were 91500 (1062.4±0.4 Ma; [61]; results applied to younger grains[62]) and/or OG1 (3465.4±0.6[63]; results applied to older grains) with Maniitsoq (337.13±0.37 Ma;[64]) and/or GJ-1 (608.53±0.37; [65]) analysed as secondary age standards. $^{206}Pb/^{238}U$ ages and $^{207}Pb/^{206}Pb$ calculated for zircon age standards, treated as unknowns, were found to be within uncertainty of the accepted value (Table EDF-7). The time-resolved mass spectra were reduced using the U_Pb_Geochronology data reduction scheme in Iolite4 (Paton et al.[66] and references therein).

2. **Trace Element Analysis**

In a separate analytical session, spots for trace element analysis were placed near locations previously analysed for Hf isotopes and age. Zircon crystals were ablated using a Resonetics RESOlution SE 193nm laser incorporating a dual volume S155 sample cell, coupled to an Agilent 8900 triple quadrupole inductively coupled plasma mass spectrometer (QQQ-ICPMS). Following two cleaning pulses and a 30s period of background analysis, samples were spot ablated for 20s at a 5Hz repetition rate using a 24µm beam and laser energy at the sample surface of 3 J cm^{-2}. An additional 15s of baseline was collected after ablation. The sample cell was flushed with ultrahigh purity He (320 mL min^{-1}) and N_2 (1.2 mL min^{-1}) and high purity Ar was employed as the plasma carrier gas, split to each mass spectrometer. The following isotopes were monitored for 0.01-0.02s each (^{27}Al, ^{31}P, ^{43}Ca, ^{45}Sc,^{49}Ti, ^{85}Rb, 88Sr, ^{89}Y, ^{91}Zr, ^{93}Nb, ^{139}La, ^{140}Ce, ^{141}Pr, ^{146}Nd, ^{147}Sm, ^{153}Eu, ^{157}Gd, ^{159}Tb, ^{163}Dy, ^{165}Ho, ^{166}Er ^{169}Tm, ^{172}Yb, ^{175}Lu, ^{178}Hf, ^{181}Ta, ^{238}U). Zircon standard GJ-1[67] was used as the primary standard to calculate elemental concentrations (^{29}Si as the internal standard element, 14.76% Si assumed in unknowns) for Ti, Y, Nb, Ce, Pr, Nd, Sm, Eu, Gd, Tb, Dy, Ho, Er, Tm, Yb, Lu and Ta. NIST 610 was utilised as the primary reference material for the remaining elements. During the time-resolved analysis, contamination resulting from inclusions and compositional zoning were monitored and only the relevant part of the signal was integrated. The trace element results for NIST 612 (secondary standard) using NIST 610 as the primary reference material indicate that the accuracy was better than 3% for all isotopes. The analytical precision was less than 7% for most elements. The time-resolved mass spectra were reduced using the Trace Elements data reduction scheme in Iolite4[66].

In Eu/Eu*–Dy/Yb space (Fig. 3a), Ordovician–Silurian grains show the lowest Eu/Eu*, indicating strong plagioclase control and crystallization from relatively shallow, plagioclase-saturated melts. Cambrian–

Ordovician grains define intermediate Eu/Eu*, whereas Carboniferous–Permian zircons extend to higher Eu/Eu* at moderate Dy/Yb, reflecting plagioclase suppression and/or more oxidizing conditions.

The U/Yb–Ce/Yb relationship (Fig. 3b) distinguishes a crustal array from a mantle-influenced array. Cambrian and Ordovician–Silurian zircons trend toward high U/Yb, indicating substantial crustal or intra-crustal contributions. In contrast, Carboniferous–Permian zircons trend toward higher Ce/Yb at low U/Yb, consistent with increasing mantle input.

In U/Yb–Nb/Yb space (Fig. 3c), most Paleozoic zircons plot above the mantle zircon array, confirming crystallization from subduction-modified arc magmas. A subset of the Carboniferous-Permian grains (in red) plot within the mantle array, consistent with the strongest mantle input among the dated suites. By contrast, the Cambrian, Ordovician–Silurian, and remaining Carboniferous–Permian populations(green) show progressively greater supra-array displacement, recording variable arc-crustal contributions.

Zircon oxybarometry and calculated melt oxidation states after Loucks et al. (2020) reveal a clear separation between suites (Fig. 3d). The Ordovician–Silurian arc grains are the most reduced, clustering near FMQ to FMQ−2 at temperatures of $\lesssim$800 °C, consistent with their evolved, crustal influenced character. The Carboniferous–Permian samples are more oxidized, extending from FMQ to FMQ+2, with the late Paleozoic suites defining the hottest population, reaching $\gtrsim$900 °C. Group medians and non-parametric comparisons confirm that the Carboniferous–Permian suites are significantly more oxidized and hotter than the Ordovician–Silurian arc.

3. **Compilation**

We compiled existing bulk rock geochemical data from the Paleozoic granitoids in Japan (EDF-2 and Suypplementary File SF13). While bulk results resulted in comparatively blurry results there are variations that show contrasting results and trends between the Cambro-Ordovician, the Ordovician-Silurian and the Carboniferous- Permian magmatism.

Declarations

Acknowledgements

DPG acknowledges funding from Spanish AEI and European Social Fund PID20212128801NA2I00 and Spanish AEI and European Social Fund “Ramón y Cajal Fellowship” RYC201920282442I. Research in the John de Laeter Centre (JdLC) GeoHistory Facility is enabled by Curtin University and the West Australian Government, and by AuScope (auscope.org.au) and the Australian Government via the National Collaborative Research Infrastructure Strategy (NCRIS). The NPII MC-ICPMS was obtained via funding from the Australian Research Council LIEF program (LE150100013). DPG acknowledges John Michael “Ozzy” Osbourne for providing the soundtrack that kept this crazy-train endeavour of a paper from going off the rails.

References

1. Moores, E. M. & Kellogg, L. H. Tectonics: 50 Years after the Revolution. *Geological Society of America Special Papers* **500**, 1–49 (2013).
2. Spencer, C. J., Roberts, N. M. W. & Santosh, M. Growth, destruction, and preservation of Earth's continental crust. *Earth-Science Reviews* **172**, 87–106 (2017).
3. Hawkesworth, C., Cawood, P., Kemp, T., Storey, C. & Dhuime, B. Geochemistry: A matter of preservation. *Science* **323**, 49–50 (2009).
4. Hawkesworth, C. J. J. & Kemp, A. I. S. I. S. Using hafnium and oxygen isotopes in zircons to unravel the record of crustal evolution. *Chemical Geology* **226**, 144–162 (2006).
5. Vezinet, A. *et al.* Growth of continental crust and lithosphere subduction in the Hadean revealed by geochemistry and geodynamics. *Nat Commun* **16**, 3850 (2025).
6. Tang, M., Rudnick, R. L., McDonough, W. F., Gaschnig, R. M. & Huang, Y. Europium anomalies constrain the mass of recycled lower continental crust. *Geology* **43**, 703–706 (2015).
7. Jagoutz, O. & Schmidt, M. W. The composition of the foundered complement to the continental crust and a re-evaluation of fluxes in arcs. *Earth and Planetary Science Letters* **371–372**, 177–190 (2013).
8. Ingalls, M., Rowley, D. B., Currie, B. & Colman, A. S. Large-scale subduction of continental crust implied by India–Asia mass-balance calculation. *Nature Geosci* **9**, 848–853 (2016).
9. Replumaz, A., Negredo, A. M., Villaseñor, A. & Guillot, S. Indian continental subduction and slab break-off during Tertiary collision. *Terra Nova* **22**, 290–296 (2010).
10. Ichikawa, H., Yamamoto, S., Kawai, K. & Kameyama, M. Estimate of subduction rate of island arcs to the deep mantle. *Journal of Geophysical Research: Solid Earth* **121**, 5447–5460 (2016).
11. Tate, G. W. *et al.* Australia going down under: Quantifying continental subduction during arc-continent accretion in Timor-Leste. *Geosphere* **11**, GES01144.1-GES01144.1 (2015).
12. Garber, J. M. *et al.* Dating Continental Subduction Beneath the Samail Ophiolite: Garnet, Zircon, and Rutile Petrochronology of the As Sifah Eclogites, NE Oman. *Journal of Geophysical Research: Solid Earth* **126**, e2021JB022715 (2021).
13. Pastor-Galán, D., Spencer, C. J., Furukawa, T. & Tsujimori, T. Evidence for crustal removal, tectonic erosion and flare-ups from the Japanese evolving forearc sediment provenance. *Earth and Planetary Science Letters* **564**, 116893 (2021).
14. Stern, C. R. Subduction erosion : Rates , mechanisms , and its role in arc magmatism and the evolution of the continental crust and mantle. *Gondwana Research* **20**, 284–308 (2011).
15. Magni, V. & Király, Á. Delamination. in *Reference Module in Earth Systems and Environmental Sciences* (Elsevier, 2020). doi:10.1016/B978-0-12-409548-9.09515-4.
16. Bird, P. Continental delamination and the Colorado Plateau. *Journal of Geophysical Research* **84**, 7561–7571 (1979).

17. Huene, R. V. & Lallemand, S. Tectonic erosion along the Japan and Peru convergent margins. *GSA Bulletin* **102**, 704–720 (1990).
18. Ichikawa, H., Kawai, K., Yamamoto, S. & Kameyama, M. Supply rate of continental materials to the deep mantle through subduction channels. *Tectonophysics* **592**, 46–52 (2013).
19. Clift, P. D., Vannucchi, P. & Morgan, J. P. Crustal redistribution, crust–mantle recycling and Phanerozoic evolution of the continental crust. *Earth-Science Reviews* **97**, 80–104 (2009).
20. Klaver, M. *et al.* Widespread slab melting in modern subduction zones. *Earth and Planetary Science Letters* **626**, 118544 (2024).
21. Shen, L., Yu, J.-H., O'Reilly, S. Y. & Griffin, W. L. Tectonic Switching of Southeast China in the Late Paleozoic. *Journal of Geophysical Research: Solid Earth* **123**, 8508–8526 (2018).
22. Gao, B., Chen, J., Huang, X., Xin, H. & Zheng, Q. Resolving the Tectonic Setting of South China in the Late Paleozoic. *Geophysical Research Letters* **49**, e2022GL099809 (2022).
23. Zhai, M. *et al.* Formation of the Northeast Asia Continent: Constrain from three geological events. *Sci. China Earth Sci.* **69**, 1456–1485 (2026).
24. Isozaki, Y., Aoki, K., Nakama, T. & Yanai, S. New insight into a subduction-related orogen: A reappraisal of the geotectonic framework and evolution of the Japanese Islands. *Gondwana Research* **18**, 82–105 (2010).
25. Isozaki, Y. *et al.* Cambrian plutonism in Northeast Japan and its significance for the earliest arc-trench system of proto-Japan: New U-Pb zircon ages of the oldest granitoids in the Kitakami and Ou Mountains. *Journal of Asian Earth Sciences* **108**, 136–149 (2015).
26. Tsujimori, T. Early Paleozoic jadeitites in Japan: An overview. *Journal of Mineralogical and Petrological Sciences* **advpub**, (2017).
27. Harada, H., Tsujimori, T., Kon, Y., Aoki, S. & Aoki, K. Nature and timing of anatectic event of the Hida Belt (Japan): Constraints from titanite geochemistry and U-Pb age of clinopyroxene-bearing leucogranite. *Lithos* **398–399**, 106256 (2021).
28. Permo-Triassic Boundary Superanoxia and Stratified Superocean: Records from Lost Deep Sea. *Science* https://www.science.org/doi/10.1126/science.276.5310.235.
29. Ganbat, A. *et al.* Crustal evolution of the Paleoproterozoic Ubendian Belt (SW Tanzania) western margin: A Central African Shield amalgamation tale. *Gondwana Research* **91**, 286–306 (2021).
30. Wallis, S. R. *et al.* The basement geology of Japan from A to Z. *Island Arc* **29**, e12339 (2020).
31. Ishiwatari, A. & Tsujimori, T. Paleozoic ophiolites and blueschists in Japan and Russian Primorye in the tectonic framework of East Asia: A synthesis. *Island Arc* **12**, 190–206 (2003).
32. Dao, N. V. *et al.* Chemical Geodynamics of Granitoid Magmatism During a Pacific-Philippine Sea Plate Transition in Southwest Japan. *Geochemistry, Geophysics, Geosystems* **27**, e2026GC012945 (2026).
33. Ito, T. *et al.* Crustal structure of southwest Japan, revealed by the integrated seismic experiment Southwest Japan 2002. *Tectonophysics* **472**, 124–134 (2009).

34. Ozawa, K., Maekawa, H., Shibata, K., Asahara, Y. & Yoshikawa, M. Evolution processes of Ordovician–Devonian arc system in the South-Kitakami Massif and its relevance to the Ordovician ophiolite pulse. *Island Arc* **24**, 73–118 (2015).
35. Ichiyama, Y., Okamoto, A., Ito, H., Tamura, A. & Morishita, T. Tectonic evolution of the Early Paleozoic proto-East Asian continental margin: Inference from Paleozoic metamorphic rocks in the South Kitakami belt, northeast Japan. *Journal of Asian Earth Sciences* **276**, 106317 (2024).
36. Collins, W. J., Belousova, E. a., Kemp, A. I. S. & Murphy, J. B. Two contrasting Phanerozoic orogenic systems revealed by hafnium isotope data. *Nature Geoscience* **4**, 333–337 (2011).
37. Jahn, B., Wu, F. & Chen, B. Granitoids of the Central Asian Orogenic Belt and continental growth in the Phanerozoic. *Earth and Environmental Science Transactions of The Royal Society of Edinburgh* **91**, 181–193 (2000).
38. Rosenbaum, G. The plate tectonic setting of mineral deposits in the New England Orogen (Australia). *Earth-Science Reviews* **276**, 105435 (2026).
39. Lundin, E. R. & Doré, A. G. Hyperextension, serpentinization, and weakening: A new paradigm for rifted margin compressional deformation. *Geology* **39**, 347–350 (2011).
40. Ashwal, L. D., Wiedenbeck, M. & Torsvik, T. H. Archaean zircons in Miocene oceanic hotspot rocks establish ancient continental crust beneath Mauritius. *Nat Commun* **8**, 14086 (2017).
41. Chapman, T., Clarke, G. L. & Daczko, N. R. The role of buoyancy in the fate of ultra-high-pressure eclogite. *Sci Rep* **9**, 19925 (2019).
42. Goes, S., Agrusta, R., van Hunen, J. & Garel, F. Subduction-transition zone interaction: A review. *Geosphere* **13**, 644–664 (2017).
43. Kimura, K. *et al.* Antiquity and tectonic lineage of Japanese Islands: New discovery of Archean–Paleoproterozoic Complex. *Earth and Planetary Science Letters* **565**, 116926 (2021).
44. Mortimer, N. *et al.* Zealandia: Earth's Hidden Continent. *GSAT* 27–35 (2017) doi:10.1130/GSATG321A.1.
45. Balázs, A., Gerya, T. & Tari, G. Presence of continental slivers in oceanic transform faults determined by rift inheritance. *Nat. Geosci.* **18**, 1303–1310 (2025).
46. Seton, M. *et al.* A Global Data Set of Present-Day Oceanic Crustal Age and Seafloor Spreading Parameters. *Geochemistry, Geophysics, Geosystems* **21**, e2020GC009214 (2020).
47. Sawada, H., Niki, S., Nagata, M. & Hirata, T. Zircon U–Pb–Hf Isotopic and Trace Element Analyses for Oceanic Mafic Crustal Rock of the Neoproterozoic–Early Paleozoic Oeyama Ophiolite Unit and Implication for Subduction Initiation of Proto-Japan Arc. *Minerals* **12**, 107 (2022).
48. Grimes, C. B. *et al.* Trace element chemistry of zircons from oceanic crust: A method for distinguishing detrital zircon provenance. *Geology* **35**, 643–646 (2007).
49. Grimes, C. B., Wooden, J. L., Cheadle, M. J. & John, B. E. "Fingerprinting" tectono-magmatic provenance using trace elements in igneous zircon. *Contrib Mineral Petrol* **170**, 46 (2015).

50. Loucks, R. R., Fiorentini, M. L. & Henríquez, G. J. New Magmatic Oxybarometer Using Trace Elements in Zircon. *J Petrology* **61**, egaa034 (2020).
51. Ferry, J. M. & Watson, E. B. New thermodynamic models and revised calibrations for the Ti-in-zircon and Zr-in-rutile thermometers. *Contrib Mineral Petrol* **154**, 429–437 (2007).

References from Online Methods

52. Defant, M. J. & Drummond, M. S. Derivation of some modern arc magmas by melting of young subducted lithosphere. *Nature* **347**, 662–665 (1990).
53. Martin, H., Smithies, R. H., Rapp, R., Moyen, J.-F. & Champion, D. An overview of adakite, tonalite–trondhjemite–granodiorite (TTG), and sanukitoid: relationships and some implications for crustal evolution. *Lithos* **79**, 1–24 (2005).
54. Woodhead, J., Hergt, J., Shelley, M., Eggins, S. & Kemp, R. Zircon Hf-isotope analysis with an excimer laser, depth profiling, ablation of complex geometries, and concomitant age estimation. *Chemical Geology* **209**, 121–135 (2004).
55. Chu N.ch. *et al.* Hf isotope ratio analysis using multi-collector inductively coupled plasma mass spectrometry: an evaluation of isobaric interference corrections. *Journal of Analytical Atomic Spectrometry* **17**, 1567–1574 (2002).
56. Patchett, P. J. & Tatsumoto, M. Hafnium isotope variations in oceanic basalts. *Geophysical Research Letters* **7**, 1077–1080 (1980).
57. Woodhead, J. D. & Hergt, J. M. A Preliminary Appraisal of Seven Natural Zircon Reference Materials for In Situ Hf Isotope Determination. *Geostandards and Geoanalytical Research* **29**, 183–195 (2005).
58. Thirlwall, M. F. & Anczkiewicz, R. Multidynamic isotope ratio analysis using MC–ICP–MS and the causes of secular drift in Hf, Nd and Pb isotope ratios. *International Journal of Mass Spectrometry* **235**, 59–81 (2004).
59. Scherer, E., Münker, C. & Mezger, K. Calibration of the Lutetium-Hafnium Clock. *Science* **293**, 683–687 (2001).
60. Blichert-Toft, J. & Albarède, F. The Lu-Hf isotope geochemistry of chondrites and the evolution of the mantle-crust system. *Earth and Planetary Science Letters* **148**, 243–258 (1997).
61. Wiedenbeck, M. *et al.* Three Natural Zircon Standards for U-Th-Pb, Lu-Hf, Trace Element and Ree Analyses. *Geostandards Newsletter* **19**, 1–23 (1995).
62. Spencer, C. J., Kirkland, C. L. & Taylor, R. J. M. Strategies towards statistically robust interpretations of in situ U–Pb zircon geochronology. *Geoscience Frontiers* **7**, 581–589 (2016).
63. Stern, R. A., Bodorkos, S., Kamo, S. L., Hickman, A. H. & Corfu, F. Measurement of SIMS Instrumental Mass Fractionation of Pb Isotopes During Zircon Dating. *Geostandards and Geoanalytical Research* **33**, 145–168 (2009).
64. Marsh, J., Jørgensen, T., Petrus, J., Hamilton, M. & Mole, D. U-Pb, Trace Element, and Hafnium Isotope Composition of the Maniitsoq Zircon: A Potential New Archean Zircon Reference Material. in

2161 (2019).

65. Jackson, S. E., Pearson, N. J., Griffin, W. L. & Belousova, E. A. The application of laser ablation-inductively coupled plasma-mass spectrometry to in situ U–Pb zircon geochronology. *Chemical Geology* **211**, 47–69 (2004).
66. Paton, C., Hellstrom, J., Paul, B., Woodhead, J. & Hergt, J. Iolite: Freeware for the visualisation and processing of mass spectrometric data. *J. Anal. At. Spectrom.* **26**, 2508–2518 (2011).
67. Liu, Y. *et al.* Reappraisement and refinement of zircon U-Pb isotope and trace element analyses by LA-ICP-MS. *Chin. Sci. Bull.* **55**, 1535–1546 (2010).

Figures

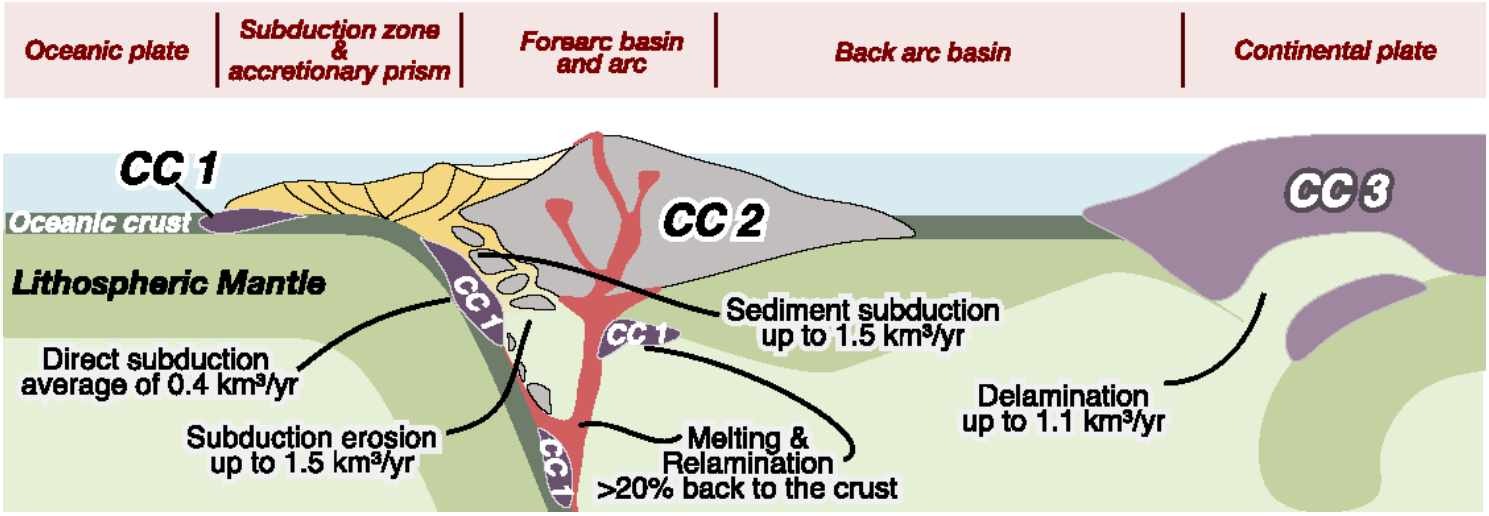


Figure 1

Mechanisms of continental crust recycling

Schematic overview of the main processes that recycle continental crust (CC) into the mantle. Numbers after CC indicate different portions of continental crust. The figure also illustrates melting and relamination processes, which return at least ~20% of the recycled material back to the crust before it can enter the mantle.

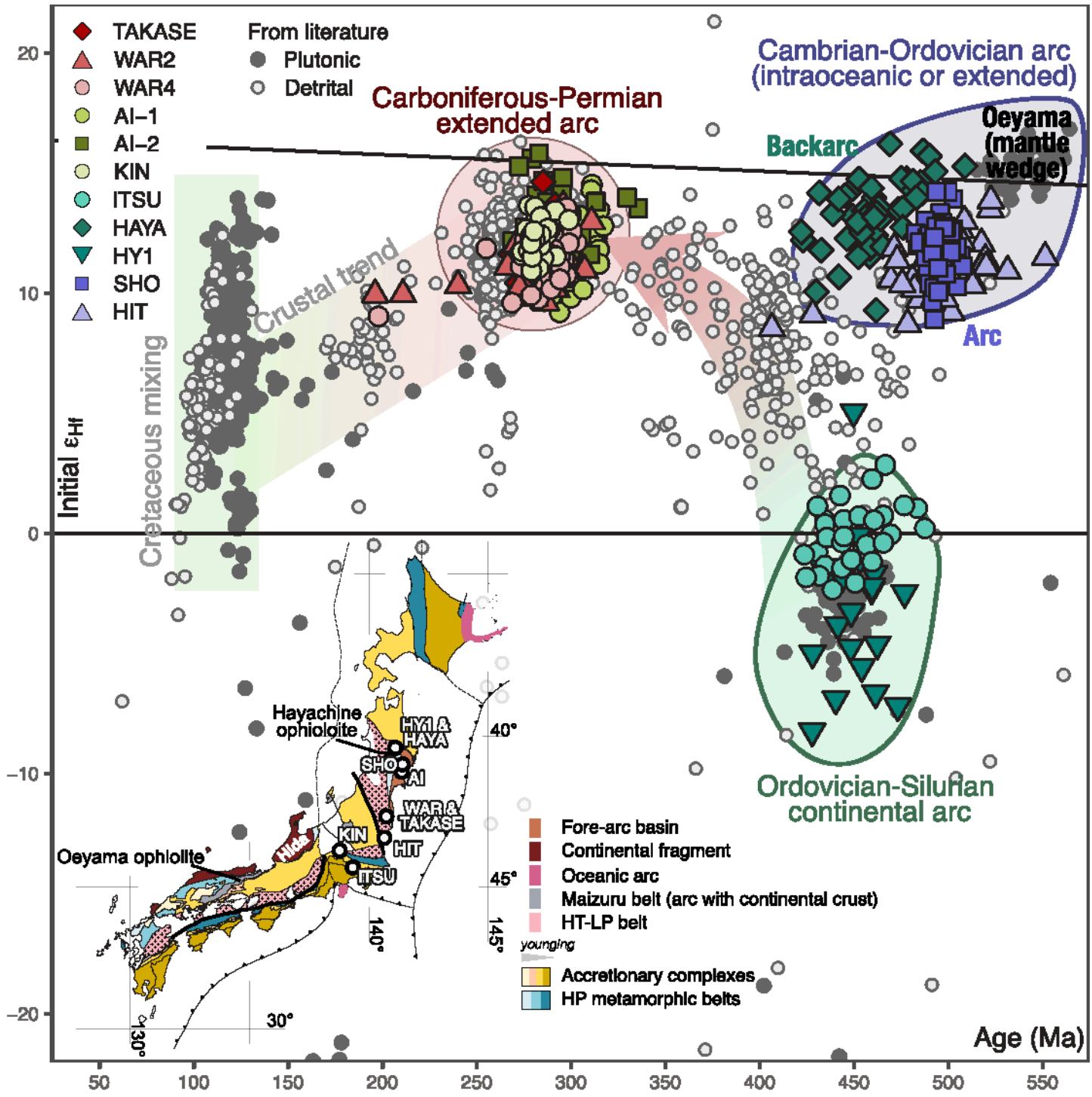


Figure 2

Sampling localities and U–Pb–Lu–Hf results

εHf values in zircon plotted against U–Pb ages for the studied samples. Grey-scale data show published results from detrital and magmatic zircons[13,47]. Inset: simplified geological map of Japan with approximate sampling locations (see Supplementary File).

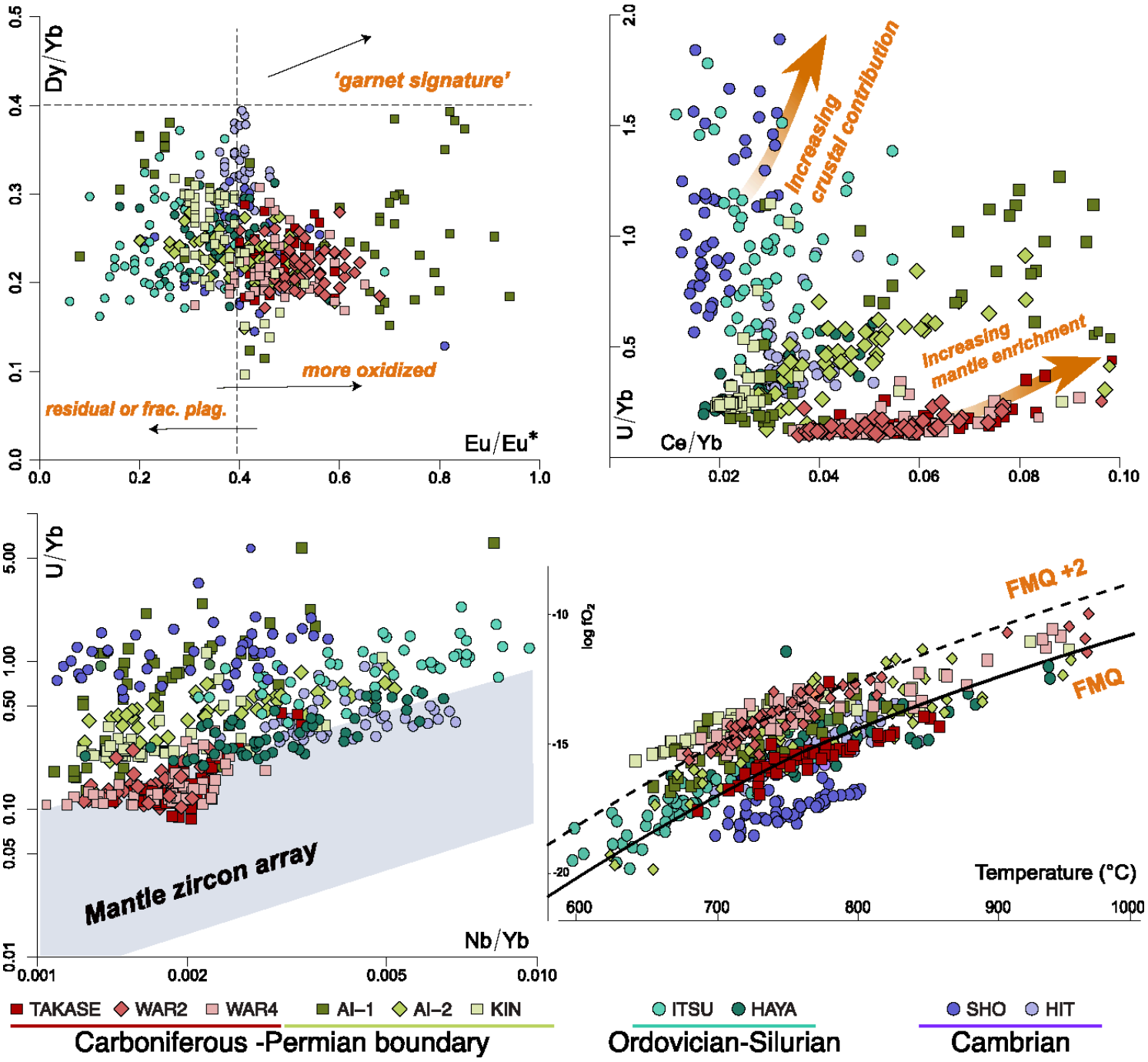


Figure 3

Zircon trace-element systematics of Paleozoic Japanese arc granitoid

(a) Eu/Eu* versus Dy/Yb. Eu/Eu* = Eu_N / √(Sm_N × Gd_N) [normalization values after McDonough and Sun, 1995]; low Eu/Eu* records plagioclase fractionation or a plagioclase-bearing residue, and elevated Dy/Yb reflects amphibole control. **(b)** U/Yb versus Ce/Yb, distinguishing crustal (high U/Yb) from oxidation-controlled (high Ce/Yb) trends[48]; **(c)** U/Yb versus Nb/Yb[49]; zircons crystallized from subduction-modified arc magmas plot above the array, whereas grains with greater mantle input fall within it. **(d)** Calculated melt oxygen fugacity (log fO_2) versus temperature, with the fayalite–magnetite–quartz buffer (FMQ) and FMQ+2 shown for reference. Oxidation states were obtained from zircon trace-element compositions[50];

crystallization temperatures are Ti-in-zircon temperatures[51] calculated assuming rutile saturation ($aTiO_2$ = 1) and $aSiO_2$ = 1 (quartz-saturated). Average propagated uncertainties are ±[*0.2*] log units in fO_2 and ± [*9*] °C in temperature.

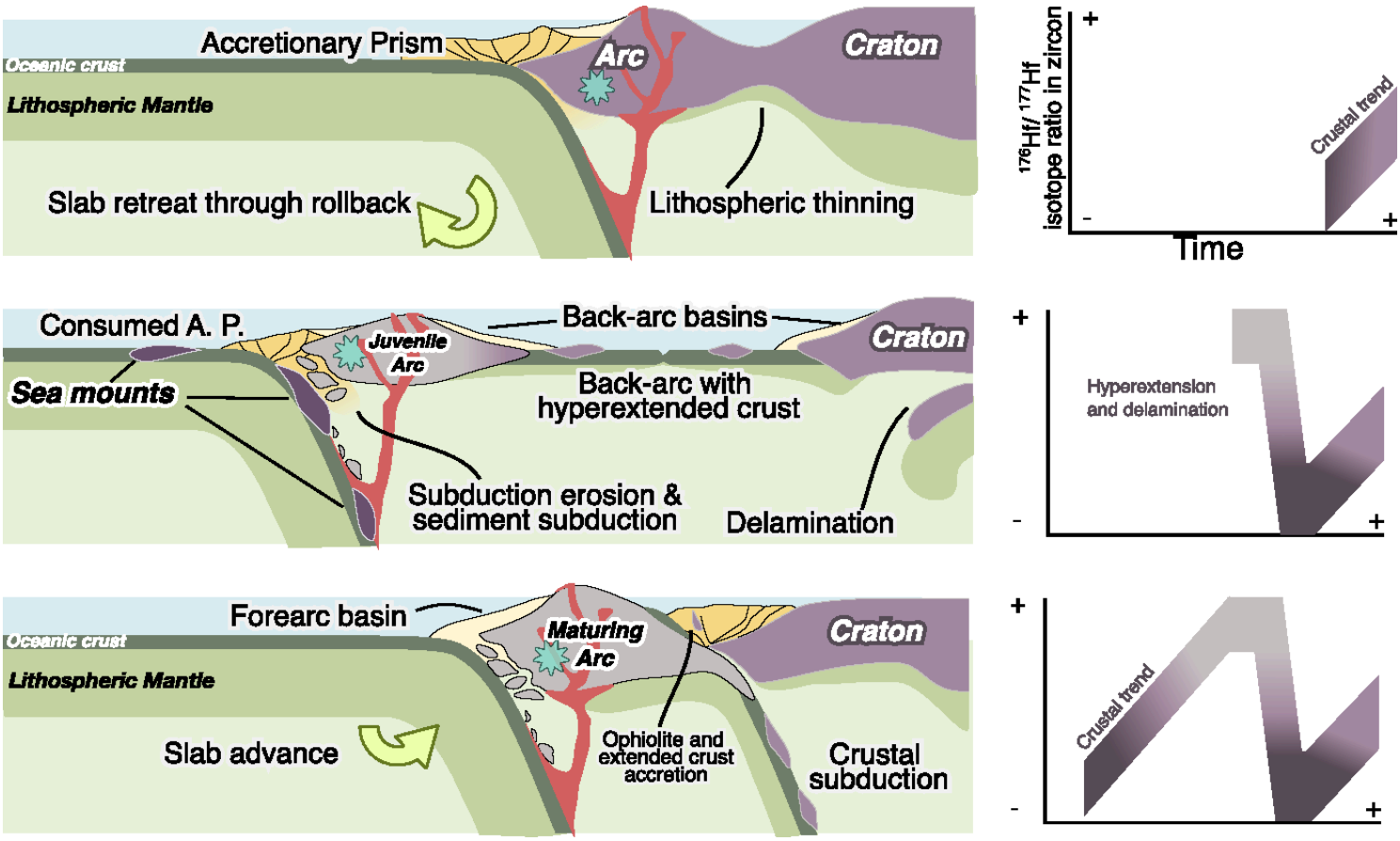


Figure 4

An effective mechanism for continental crust recycling

Conceptual model illustrating three stages of the proposed recycling mechanism. Top: continental arc prior to slab rollback. Middle: rollback-driven extension, including tectonic erosion (for example, by subduction of seamounts or plateaus) and delamination in the cratonic interior. Bottom: slab advance and subduction of the back-arc domain, including previously stretched continental crust. Polarities are schematic and not intended to represent a specific case.

Supplementary Files

This is a list of supplementary files associated with this preprint. Click to download.

- EDF4.pdf
- EDF5.xlsx
- EDF2.pdf

- EDF6.docx
- EDF7.docx
- EDF3.pdf
- SF13.xlsx
- EDF1.pdf
- Supplementarymaterial.pdf
- ExtendedData.docx